

Analytical Singular Value Decomposition of infrared image sequences: microcrack detection on ceramic composites under mechanical stresses

Matthieu Bamford *, Jean Christophe Batsale

TREFLE-ENSAM, UMR 8508 CNRS, Esplanade des Arts et Métiers, 33405 Talence, France

Received 29 May 2007; accepted after revision 17 December 2007

Available online 21 March 2008

Presented by Michel Combarous

Abstract

In this Note, infrared image sequences of a SiC_f/SiC composite excited with a uniform heat pulse are processed using a modal approach. A new analytical integral transform (called analytical SVD or ASVD) inspired by the classical Singular Value Decomposition is developed and implemented on the raw experimental data. The second resulting spatial mode (out of a thousand) yielded by the ASVD provides, without further processing, a 2D mapping of the normalized local transverse diffusivity variations around a nominal value. Such mapping yields information on the inner structure of the material, and can be used to reveal the presence of voids inside the medium. This method is thus implemented on a tensile testing machine, to detect microcracks in a SiC_f/SiC composite sample under mechanical stress in almost real time. *To cite this article: M. Bamford, J.C. Batsale, C. R. Mecanique 336 (2008).*

© 2008 Académie des sciences. Published by Elsevier Masson SAS. All rights reserved.

Résumé

Décomposition en Valeurs Singulières Analytique de séquences d'images infrarouges : détection de microfissures sur des composites céramiques sous contraintes mécaniques. Dans cette étude, des séquences d'images infrarouges obtenues en filmant un composite SiC_f/SiC excité par un flash uniforme sont traitées avec une approche modale. Une nouvelle transformation intégrale analytique (appelée SVD analytique ou ASVD) inspirée de la Décomposition en Valeurs Singulières classique est mise au point et appliquée aux données expérimentales brutes. Le deuxième mode spatial (parmi un millier) issu de l'ASVD fournit sans traitement supplémentaire une cartographie 2D normalisée des variations locales de diffusivités transverses autour d'une valeur nominale. De telles cartographies nous renseignent sur la structure interne du matériau, et peuvent être utilisées en particulier pour révéler la présence de cavités sous la surface. Cette méthode est donc implémentée sur un banc de traction, pour détecter en temps réel d'éventuelles microfissures sur un échantillon de composite SiC_f/SiC soumis à une importante contrainte mécanique uniaxiale. *Pour citer cet article : M. Bamford, J.C. Batsale, C. R. Mecanique 336 (2008).*

© 2008 Académie des sciences. Published by Elsevier Masson SAS. All rights reserved.

Keywords: Heat transfer; Analytical Singular Value Decomposition; Flash method; Infrared camera; Transverse diffusivity distribution; Ceramic composite

* Corresponding author.

E-mail address: matthieu.bamford@bordeaux.ensam.fr (M. Bamford).

Mots-clés : Transferts thermiques ; Décomposition en Valeurs Singulières Analytique ; Méthode flash ; Camera infrarouge ; Cartographie de diffusivités transverses ; Composite céramique

1. Introduction

Image sequences from a transient state provided by infrared cameras are often used for Non Destructive Testing (NDT) of composites [1]. Such testing is either done by computing thermophysical properties distributions of the composite [2]—by associating infrared sequences with physical models of heat transfer—or by qualitatively interpreting spatial modes resulting from the decomposition of the raw infrared sequences, using orthogonal transforms, such as Singular Value Decompositions—SVD—for example [3].

Usual inversion methods implemented so far to retrieve parameter fields are generally based on the local implementation of finite difference schemes at each pixel—or node—[4]; therefore they are referred to as ‘nodal approaches’. Some difficulties associated with these nodal approaches are the local lack of sensitivity to the parameters studied, and the need to collect and manipulate a great amount of data to extract only little significant information. As a consequence, simple and fast modal decompositions such as the SVD are preferably applied to infrared sequences to perform real time NDT of heterogeneous media. In the literature, this approach is referred to as the Principal Component Analysis (PCA) [5] and is confined to qualitative studies because it lacks some physical content.

In this study, a new simple analytical integral transform inspired by the SVD is developed. This Analytical SVD (ASVD) is implemented on raw infrared sequences of a composite sample excited with a flash lamp. Due to a better understanding of the simple ASVD computation procedure (as compared to the SVD), quantitative physical information on the inner structure of the composite sample is obtained from a straightforward observation of its modes. Effective 2D distributions of the normalized local transverse diffusivity variations around a nominal value of a composite sample under tensile testing are provided by the second spatial ASVD mode and related to the presence of microcracks in the composite [6], thus demonstrating that ASVD—coupled with an infrared camera and a flash device—can be used as a local damage indicator to study SiC_f/SiC composite samples under tensile testing.

2. Experimental setup

The ‘Flash’ method is associated here with an ‘ORION’ infrared camera (CEDIP) whose properties are described in [7]. The SiC_f/SiC sample dimensions are $l = 200 \times 10^{-3}$ m, $L = 16 \times 10^{-3}$ m, and $e = 2 \times 10^{-3}$ m. The composite is placed between the flash lamp and the infrared camera (Fig. 1).

The ‘flash’ excitation is performed on the front face of the sample, and the rear face temperature distribution is filmed with an infrared camera. The resulting infrared sequences are processed to estimate normalized mappings of the local transverse diffusivity variations of the material.

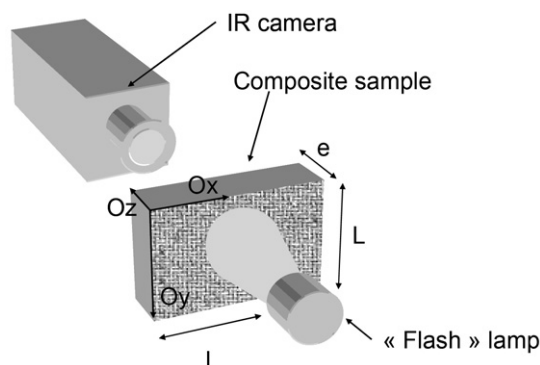


Fig. 1. Scheme of the ‘flash’ experiment.

Fig. 1. Schéma du dispositif ‘flash’.

3. Simplified heat transfer model

In the case of a uniform flash excitation, heat transfer inside the medium is considered 1D in the O_z direction and the in-plane diffusion is neglected. Even though such configuration is experimentally difficult to realize, it remains a good approximation for thin samples at short times—which is the case here since the thickness e of the sample is small as compared to its length l . The rear face temperature distribution can thus be expressed as the following product of functions [8]:

$$T(x, y, e, t) = T_{\max}(x, y) \cdot f[t/\tau(x, y)] \quad (1)$$

where $T_{\max}(x, y)$ is the maximum temperature reached at position (x, y) and is related to the local flash intensity, and $\tau(x, y)$ is a local transverse characteristic time defined by

$$\tau(x, y) = e^2/a_z(x, y) \quad (2)$$

with $a_z(x, y)$ the local transverse diffusivity. Using expression (1), a Taylor's development of the temperature at each pixel can be performed around the nominal value $\tau_0 = e^2/a_z^0$

$$T(x, y, e, t) \approx T_{\max}(x, y) \cdot [f(t/\tau_0) + (\tau - \tau_0)(x, y) \cdot \partial f(t/\tau_0)/\partial \tau_0] \quad (3)$$

and with

$$\{T\}_{x,y}(t) = \left[\int_0^L \int_0^l T(x, y, e, t) dx dy \right] / lL \quad (4)$$

where $\{\cdot\}_{x,y}$ denotes a space average; relation (3) becomes

$$T(x, y, e, t) \approx T_{\max}(x, y) \cdot [\{T/T_{\max}\}_{x,y}(t) + (\tau - \tau_0)(x, y) \cdot \partial [\{T/T_{\max}\}_{x,y}(t)]/\partial \tau_0] \quad (5)$$

Under the assumption that $\{T/T_{\max}\}_{x,y} \approx \{T\}_{x,y}/\{T_{\max}\}_{x,y}$,—meaning that the heat flux induced by the flash lamp is spatially rather uniform, and that the sample is slightly heterogeneous—it yields:

$$T(x, y, e, t) \approx B(x, y) \cdot [\{T\}_{x,y}(t) + (\tau - \tau_0)(x, y) \cdot \partial [\{T\}_{x,y}(t)]/\partial \tau_0] \quad (6)$$

with $B(x, y) = T_{\max}(x, y)/\{T_{\max}\}_{x,y}$

The resolution of Eq. (6) requires an accurate definition of the sensitivity function $\partial \{T\}_{x,y}/\partial \tau_0$, yet in most experimental configurations such model is not available. In previous studies ([8]) this function was replaced by $t \cdot \partial \{T\}_{x,y}/\partial t$; in this paper a new simple and robust way to compute $\partial \{T\}_{x,y}/\partial \tau_0$ is proposed using the Analytical SVD.

4. Analytical SVD algorithm

Given a sequence $\{T_k(x, y)\}_{k=1..N} = \{T(x, y, e, t_k)\}_{k=1..N}$ of N measured temperature distributions— (x, y) being the space variables and t_k corresponding to the k th time step—it is possible to implement a recursive algorithm that performs successive approximations as follows

$$\psi^1(x, y, t) = T(x, y, e, t) \quad \text{initialization} \quad (7)$$

where $\psi^n(x, y, t)$, $n \in \llbracket 1, N \rrbracket$, corresponds to 'residues' between a function and its approximation. When $n = 1$, the residues are equal to the studied function—i.e. the temperature distribution $T(x, y, e, t)$ here. Each successive approximation is performed by decomposing $\psi^n(x, y, t)$ into a product of separable functions obtained by 'projecting' $\psi^n(x, y, t)$ over both space and time. The normalized projection of ψ^n over space is called U^n and is computed as follows:

$$U^n(x, y) = \{\psi^n \cdot \{\psi^n\}_{x,y}\}_t(x, y) / \|\{\psi^n \cdot \{\psi^n\}_{x,y}\}_t\|_{x,y}, \quad n \in \llbracket 1, N \rrbracket \quad (8)$$

Notations are simplified by introducing the space and time averages i.e. $\{\cdot\}_{x,y}$ and $\{\cdot\}_t$, and the space and time L^2 norms i.e. $\|\cdot\|_{x,y}$ and $\|\cdot\|_t$. The normalized projection of ψ^n over time is called V^n and is computed as follows

$$V^n(t) = \{\psi^n \cdot U^n\}_{x,y}(t) / \|\psi^n \cdot U^n\|_t, \quad n \in \llbracket 1, N \rrbracket \quad (9)$$

The ‘norm’ of the resulting decomposition of ψ^n is then given by

$$\lambda_n = \{ \{ \psi^n \cdot V^n \}_t \cdot U^n \}_{x,y}, \quad n \in \llbracket 1, N \rrbracket \tag{10}$$

and a possible separable approximation of ψ^n is φ^n given by

$$\psi^n(x, y, t) \approx \varphi^n(x, y, t) = \lambda_n \cdot U^n(x, y) \cdot V^n(t), \quad n \in \llbracket 1, N \rrbracket \tag{11}$$

The residues of this approximation are simply

$$\psi^{n+1}(x, y, t) = \psi^n(x, y, t) - \varphi^n(x, y, t), \quad n \in \llbracket 1, N \rrbracket \tag{12}$$

Finally the whole sequence of temperature distributions can be written as

$$T(x, y, e, t) = \sum_{k=1}^N \lambda_k \cdot U_k(x, y) \cdot V_k(t)^T + \psi^{N+1}(x, y, t) \tag{13}$$

When $\psi^{N+1} \approx 0$, this formulation is exactly the same as for the classical SVD. Besides, if the sequence $\{\lambda_n\}_{n \in \llbracket 1, N \rrbracket}$ is rapidly decreasing, then only the first few modes of the decomposition are significant, which appears to be very suitable for data compression. Both conditions are satisfied when the following criteria are respected:

$$\begin{aligned} \{U_k \cdot U_l\}_{x,y} &= \delta_k^l = \{V_k \cdot V_l\}_t \\ \{U_i\}_{x,y} \neq 0 \quad \text{and} \quad \lambda_i^2 &\gg \sum_{k=i+1}^N \lambda_k^2 \cdot [\{U_k\}_{x,y} / \{U_i\}_{x,y}]^2, \quad i \in \llbracket 1, N - 1 \rrbracket \end{aligned} \tag{14}$$

Here δ_k^l designates the Kronecker symbol. These conditions are always fulfilled in the examples treated. However, the most interesting feature of this analytical transform is that it provides decompositions similar to that obtained with the SVD, with less computation time, and a more simple algorithm allowing a better understanding of the physical meaning of its resulting modes.

This can be illustrated using simulated data representing the rear face temperature response of a 2D heterogeneous medium to a spatially uniform flash. The simulated medium is depicted in Fig. 2 along with the resulting temperature profiles in Fig. 3:

The simulated rear face temperature profiles, presented in Fig. 3, are decomposed using both the standard SVD and the Analytical SVD (ASVD). The resulting singular values are plotted Fig. 4 to visualize their rapid decay. The quadratic distances between the modes obtained with both decompositions are computed, Fig. 5, to show the similarities between them.

For both decompositions, the singular values decrease sharply with the mode index (Fig. 4). Besides, the modes yielded by each decomposition are rather similar, as illustrated by the low quadratic distances between them (Fig. 5).

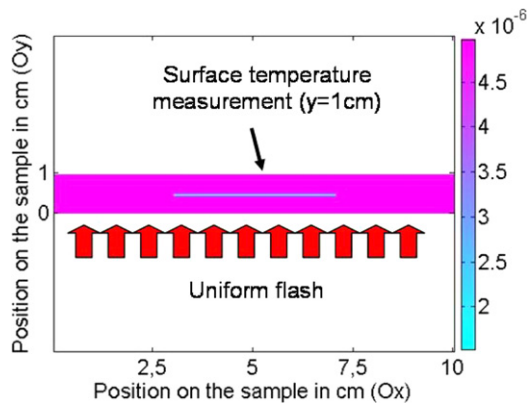


Fig. 2. Scheme of the simulated 2D medium.
Fig. 2. Schéma du milieu 2D simulé.

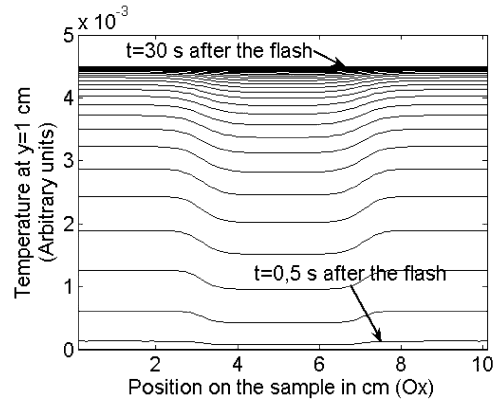


Fig. 3. Temperature profiles, simulated using the medium described in Fig. 2.
Fig. 3. Profils de température simulés à partir du milieu de la Fig. 2.

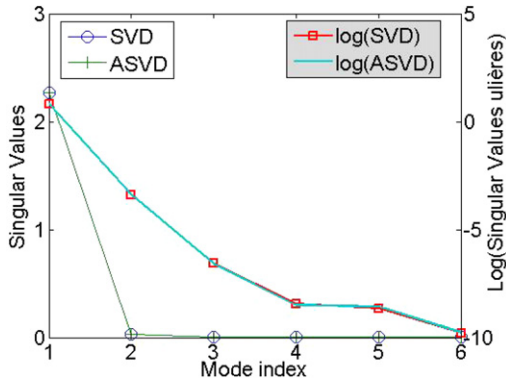


Fig. 4. Singular values from both SVD and ASVD of the data simulated in Fig. 3.

Fig. 4. Valeurs singulières issues de la SVD et de la SVDA du signal présenté Fig. 3.

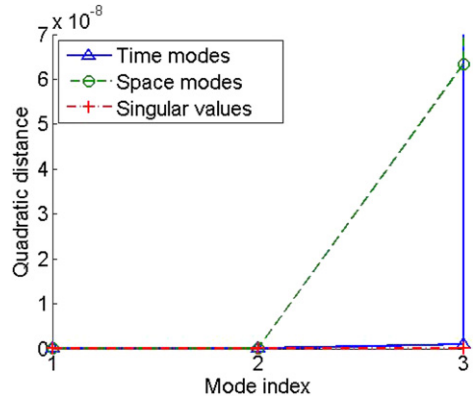


Fig. 5. Quadratic distances between SVD and ASVD of the data simulated in Fig. 3.

Fig. 5. Distances quadratiques entre les modes de la SVD et de la SVDA du signal présenté Fig. 3.

In addition, the computation time required for the ASVD is at least ten times inferior to that needed by the standard SVD on the examples treated.

The exposed similarities—between SVD and ASVD—allow us to study the physical significance of the modes yielded by the ASVD to finally explain—by analogy—why SVD allows for thermal NDE of composites.

5. Full diffusivity fields measurement using the Analytical SVD

By setting $n = 1$ in expression (7) and considering relation (6), it can be shown that

$$U^1(x, y) = \{T \cdot \mu_1\}_t(x, y) / \|\{T \cdot \mu_1\}_t\|_{x,y}, \quad V^1(t) = \{T \cdot v_1\}_{x,y}(t) / \|\{T \cdot v_1\}_{x,y}\|_t \tag{15}$$

with $\mu_1(t)$ and $v_1(x, y)$ the following time and space weighting coefficients:

$$\mu_1 = \{T\}_{x,y} / \{\{T\}_{x,y}\}_t, \quad v_1 = \{T\}_t / \{\{T\}_{x,y}\}_t \Rightarrow \{\mu_1\}_t = 1, \quad \{v_1\}_{x,y} = 1, \quad \mu_1 \geq 0, \quad v_1 \geq 0 \tag{16}$$

In addition, looking at relation (6),

$$\begin{aligned} \{T\mu_1\}_t &\approx \{B(x, y) \cdot [\{T\}_{x,y}(t) + (\tau - \tau_0)(x, y) \cdot \partial[\{T\}_{x,y}(t)]/\partial\tau] \cdot \{T\}_{x,y}(t)\}_t / \{\{T\}_{x,y}\}_t \\ \{Tv_1\}_{x,y} &\approx \{B(x, y) \cdot [\{T\}_{x,y}(t) + (\tau - \tau_0)(x, y) \cdot \partial[\{T\}_{x,y}(t)]/\partial\tau] \cdot v_1(x, y)\}_{x,y} \end{aligned} \tag{17}$$

which means that

$$\begin{aligned} \{T\mu_1\}_t &\approx B(x, y) \cdot [\{\{T\}_{x,y}^2\}_t + (\tau - \tau_0)(x, y) \cdot \{\partial[\{T\}_{x,y}(t)]/\partial\tau \cdot \{T\}_{x,y}\}_t] / \{\{T\}_{x,y}\}_t \\ \{Tv_1\}_{x,y} &\approx \{T\}_{x,y}(t) \cdot \{B(x, y) \cdot v_1(x, y)\}_{x,y} + \partial[\{T\}_{x,y}(t)]/\partial\tau \cdot \{B(x, y) \cdot (\tau - \tau_0)(x, y) \cdot v_1(x, y)\}_{x,y} \end{aligned} \tag{18}$$

and since

$$\begin{aligned} |(\tau - \tau_0)(x, y) \cdot \{\partial[\{T\}_{x,y}(t)]/\partial\tau \cdot \{T\}_{x,y}\}_t| &\ll \{\{T\}_{x,y}^2\}_t = \|\{T\}_{x,y}\|_t^2 \\ |\partial[\{T\}_{x,y}(t)]/\partial\tau \cdot \{B(x, y) \cdot (\tau - \tau_0)(x, y) \cdot v_1(x, y)\}_{x,y}| &\ll \{T\}_{x,y}(t) \cdot \{B(x, y) \cdot v_1(x, y)\}_{x,y} \end{aligned} \tag{19}$$

it yields that

$$\begin{aligned} \{T\mu_1\}_t &\approx B \cdot \|\{T\}_{x,y}\|_t^2 \cdot [1 + (\tau - \tau_0) \cdot \{\partial[\{T\}_{x,y}]/\partial\tau \cdot \{T\}_{x,y}\}_t / \|\{T\}_{x,y}\|_t^2] / \{\{T\}_{x,y}\}_t \\ \{Tv_1\}_{x,y} &\approx \{T\}_{x,y} \cdot \{B \cdot v_1\}_{x,y} \left[1 + \frac{\partial[\{T\}_{x,y}]/\partial\tau \cdot \{B \cdot (\tau - \tau_0) \cdot v_1\}_{x,y}}{\{T\}_{x,y} \cdot \{B \cdot v_1\}_{x,y}} \right] \end{aligned} \tag{20}$$

and

$$\begin{aligned} \{T\mu_1\}_t &\approx B \cdot \|\{T\}_{x,y}\|_t^2 \cdot [1 + o(1)] / \{\{T\}_{x,y}\}_t = B \cdot \|\{T\}_{x,y}\|_t^2 / \{\{T\}_{x,y}\}_t + o(B \cdot \|\{T\}_{x,y}\|_t^2 / \{\{T\}_{x,y}\}_t) \\ \{Tv_1\}_{x,y} &\approx \{T\}_{x,y} \cdot \{B \cdot v_1\}_{x,y} \cdot [1 + o(1)] = \{T\}_{x,y} \cdot \{B \cdot v_1\}_{x,y} + o(\{T\}_{x,y} \cdot \{B \cdot v_1\}_{x,y}) \end{aligned} \tag{21}$$

This leads to

$$\begin{aligned} \| \{T \mu_1\}_t \|_{x,y} &\approx \| B \|_{x,y} \cdot \| \{T\}_{x,y} \|_t^2 / \{ \{T\}_{x,y} \}_t \\ \| \{T v_1\}_{x,y} \|_t &\approx \| \{T\}_{x,y} \|_t \cdot \{ B \cdot v_1 \}_{x,y} \end{aligned} \tag{22}$$

So that finally

$$\begin{aligned} U^1 &= \{T \mu_1\}_t / \| \{T \cdot \mu_1\}_t \|_{x,y} \approx B / \| B \|_{x,y} + o(B / \| B \|_{x,y}) \approx T_{\max} / \| T_{\max} \|_{x,y} + o(T_{\max} / \| T_{\max} \|_{x,y}) \\ V^1 &= \{T v_1\}_{x,y} / \| \{T v_1\}_{x,y} \|_t \approx \{T\}_{x,y} / \| \{T\}_{x,y} \|_t + o(\{T\}_{x,y} / \| \{T\}_{x,y} \|_t) \end{aligned} \tag{23}$$

where U^1 and V^1 are the first space and time modes yielded by the ASVD of T . Relation (23) emphasizes the fact that U^1 gives a close approximation to the normalized local maximum temperature distribution $T_{\max} / \| T_{\max} \|_{x,y}$ whereas V^1 is an approximation to the normalized time evolution of the averaged rear face temperature $\{T\}_{x,y} / \| \{T\}_{x,y} \|_t$. As a conclusion, the first ASVD mode accounts for the first order of Taylor’s development. At this stage, it is thus possible to write

$$\psi^2 = T - \lambda_1 \cdot U^1 \cdot V^1 \approx B \cdot (\tau - \tau_0) \cdot \partial \{T\}_{x,y} / \partial \tau \tag{24}$$

and thus

$$\{ \psi^2 \cdot \{ \psi^2 \}_{x,y} \}_t \approx \{ B \cdot (\tau - \tau_0) \}_{x,y} \cdot B \cdot (\tau - \tau_0) \cdot \{ [\partial \{T\}_{x,y} / \partial \tau]^2 \}_t \tag{25}$$

so that, given the definitions of U^1 and U^2

$$U^2 \propto U^1 \cdot (\tau - \tau_0) \tag{26}$$

It appears that normalized local characteristic time variations can be observed by considering U^2 / U^1 without further computation. For spatially uniform flashes with slightly heterogeneous samples, the first spatial mode U^1 is slowly varying and U^2 is a normalized approximation to $(\tau - \tau_0) / \tau_0$ (e.g. it is an approximation to $(\tau - \tau_0) / \| \tau - \tau_0 \|_{x,y}$). This point can be illustrated Fig. 6 by comparing the exact characteristic time variations profile of the medium presented in Fig. 2 with the 2nd spatial mode U^2 of the ASVD, computed with the simulated data presented in Fig. 3.

It appears in Fig. 6 that the second spatial mode yielded by the ASVD is a good approximation to the characteristic time relative variations profile.

However, it must be noticed that when performing the ASVD on a unique set of initial data, the signs of the resulting both U^2 and V^2 can either be simultaneously negative or simultaneously positive—without changing the

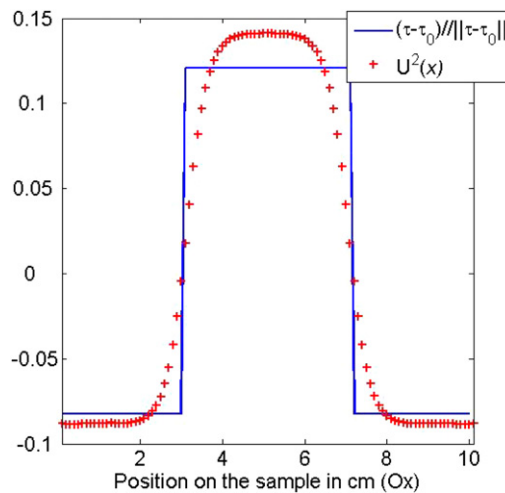


Fig. 6. Comparison between the exact profile of the relative characteristic time variations, and the 2nd spatial mode provided by the ASVD of the data depicted in Fig. 3.

Fig. 6. Comparaison entre le profil exact des variations relatives de temps caractéristique, et le second mode spatial issu de la SVDA des données représentées Fig. 3.

product $U^2 \cdot V^2$ —due to the ASVD algorithm (the same phenomenon occurs with SVD). It is thus necessary to multiply U^2 by the sign of the scalar product $\{V^2 \cdot t \cdot \partial\{T\}_{x,y}/\partial t\}_t$, to make sure the interpretation of U^2 is not biased. Besides, using the following notations

$$(\tau - \tau_0)/\tau_0 = \Delta\tau/\tau_0 \quad \text{with } \Delta\tau = e^2 \cdot \Delta(1/a_z) = -e^2 \cdot \Delta a_z/(a_z^0)^2 \tag{27}$$

it can be shown that

$$\Delta\tau/\tau_0 = -\Delta a_z/a_z^0 \tag{28}$$

so that eventually, U^2 can be considered as a normalized approximation to the transverse diffusivity relative variations distribution $-\Delta a_z/a_z^0$.

Such considerations allow to apply the ASVD to infrared sequences obtained with the experimental device presented Fig. 1, in order to extract normalized distributions of the characteristic time relative variations from a composite sample under tensile testing.

6. Experimental results

Using the experimental setup presented in Fig. 1, infrared sequences of a SiC_f/SiC composite under tensile testing are obtained for increasing mechanical stresses. Examples of obtained infrared images are presented in Fig. 7. The ASVD is applied to each sequence and the evolution of the resulting second modes with respect to the mechanical stresses is studied in Fig. 8.

The resulting mappings reveal the presence of transverse diffusivity variations. The dark areas correspond to low transverse diffusivities, and thus presumably to damaged areas. For ‘low’ mechanical stresses (50 to 100 MPa) a single small area on the left part of the sample concentrates all the microcracks, this location is assumed to be a moot point of the composite even before tensile testing. For higher stresses (150 to 200 MPa) the microcracks appear homogeneously throughout the surface of the sample, at 250 MPa microcracks cross the sample perpendicularly to the traction direction which is in agreement with the damage process described in [9]. These cracks prefigure the ultimate failure that happens at 275 MPa.

Finally, simple ASVD-based NDT allows one to visualise microscopically in depth cracks that would usually require more sophisticated means of characterization such as X-rays or a chemical attack of the damaged composite. As an illustration the real size of the crack responsible for the ultimate failure can be seen on Fig. 9, and compared to the size of the blue area on the right part of Fig. 8.

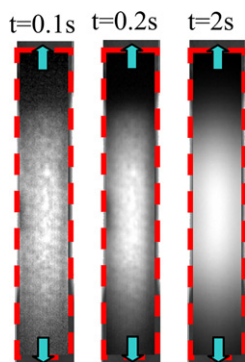


Fig. 7. Rear face infrared images of the sample at different times after the flash.

Fig. 7. Images infrarouges de la face arrière d’une éprouvette composite à différents instants après le flash.

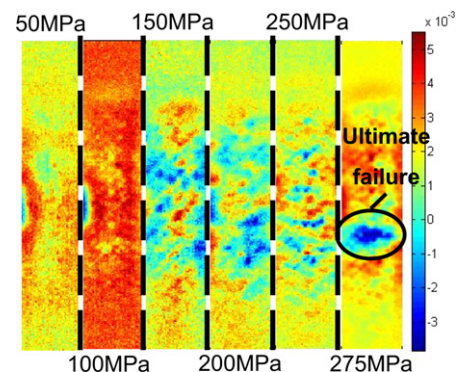


Fig. 8. Evolution of the Second ASVD modes with respect to mechanical stress.

Fig. 8. Evolution des deuxièmes modes issus de l’ASVD en fonction de la contrainte mécanique.

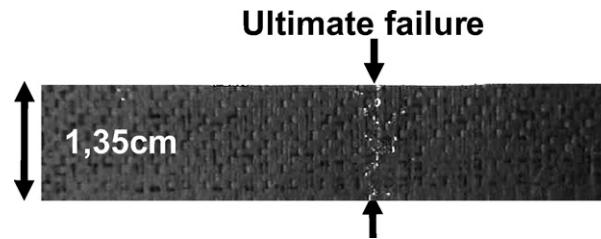


Fig. 9. Real microscopic size of the cracks that cause the large diffusivity variations depicted in Fig. 8.

Fig. 9. Taille réelle microscopique des fissures à l'origine des larges variations de diffusivités représentées Fig. 8.

7. Conclusions

A new original analytical integral transform is developed to assess normalized thermal diffusivity distributions of a heterogeneous medium using a flash device coupled with an infrared camera. This modal approach is used to study SiC_f/SiC composites under tensile testing for increasing stress.

Effective normalized local diffusivity variations are measured and related to the presence of microcracks in the composite thus demonstrating the convenience of this method for damage evaluation. The small computation time required by the simple ASVD-based estimation procedure and its roughness—since no matrix inversion is needed—are put forward. Such assets associated with the simplicity of the experimental setup—as compared to other standard means devoted to microcracks characterization—allow performing in situ and almost real time NDT on composites during tensile testing.

In this Note, the role of the second mode yielded by the ASVD in assessing normalized transverse diffusivity distributions is highlighted. It must be noted that further works shall address the issue of obtaining complementary physical information by observing other ASVD modes; the estimation of exact transverse and longitudinal diffusivity profiles using the same heat transfer models as presented here associated with nodal and modal strategies is also under discussion.

Acknowledgements

The authors acknowledge the LCTS laboratory, Jacques Lamon, Olivier Loseille, and Bruno Humez who provided the composites and the tensile testing machine, and helped with the experiments.

References

- [1] D. Balageas, P. Delpech, D. Boscher, A. Deom, New developments in stimulated infrared thermography applied to non destructive evaluation of laminates, in: *Review of Progress in QNDE*, vol. 10A, Plenum Press, New York, 1991, pp. 1073–1081.
- [2] J.C. Krapez, L. Spagnolo, M. Frieß, H.P. Maier, G. Neuer, Measurement of in-plane diffusivity in non-homogeneous slabs by applying flash thermography, *Int. J. Thermal Sci.* 43 (2004) 967–977.
- [3] N. Rajic, Principal component thermography for flaw contrast enhancement and flaw depth characterisation in composite structures, *Composite Structures* 58 (4) (2002) 521–528.
- [4] M. Bamford, J.C. Batsale, D. Reungoat, O. Fudym, Two dimensional velocity and diffusion mappings in the case of three dimensional transient diffusion: “Flash” method and infrared images sequences analysis, in: *8th Conf. on Quantitative Infrared Thermography, QIRT 2006*, Padova, Italy, June 2006, pp. 27–30.
- [5] X. Chen, P.J. Flynn, K.W. Bowyer, PCA-based face recognition in infrared imagery: baseline and comparative studies, in: *AMFG 2003, IEEE International Workshop on Analysis and Modeling of Faces and Gestures*, 17 Oct. 2003, pp. 127–134.
- [6] J. Sun, Evaluation of ceramic matrix composites by thermal diffusivity imaging, *Int. J. Appl. Ceram. Technol.* 4 (1) (2007) 75–87.
- [7] M. Bamford, J.C. Batsale, O. Fudym, Singular Value Decomposition of infrared image sequences. Application to thermal diffusivity profile estimation after a “Flash” excitation, in: *Inverse Problems, Design and Optimization Symposium, IPDO 2007*, Miami, USA, April 16–20, 2007.
- [8] D. Mourand, J. Gounod, J.C. Batsale, New sequential method to process noisy temperature response from flash experiment measured by infrared camera, *Rev. Sci. Instrum.* 69 (3) (1998) 1437–1440.
- [9] X. Aubard, J. Lamon, Model of nonlinear mechanical behavior of 2D SiC–SiC chemical vapor infiltration composites, *J. Amer. Ceram. Soc.* 77 (8) (1994) 2118–2126.